Video Article

Solvothermal Synthesis of MIL-96 and UiO-66-NH_2 on Atomic Layer Deposited Metal Oxide Coatings on Fiber Mats

Heather F. Barton[1], Alexandra K. Davis[1], Dennis T. Lee[1], Gregory N. Parsons[1]

[1]Department of Chemical and Biomolecular Engineering, North Carolina State University

Correspondence to: Heather F. Barton at hfbarton@ncsu.edu

URL: https://www.jove.com/video/57734
DOI: doi:10.3791/57734

Keywords: Chemistry, Issue 136, Metal-organic frameworks, atomic layer deposition, solvothermal

Date Published: 6/13/2018

Citation: Barton, H.F., Davis, A.K., Lee, D.T., Parsons, G.N. Solvothermal Synthesis of MIL-96 and UiO-66-NH_2 on Atomic Layer Deposited Metal Oxide Coatings on Fiber Mats. *J. Vis. Exp.* (136), e57734, doi:10.3791/57734 (2018).

Abstract

Metal-organic frameworks (MOFs), which contain reactive metal clusters and organic ligands allowing for large porosities and surface areas, have proven effective in gas adsorption, separations, and catalysis. MOFs are most commonly synthesized as bulk powder, requiring additional processes to adhere them to functional devices and fabrics that risk decreasing the powder porosity and adsorption capacity. Here, we demonstrate a method of first coating fabrics with metal oxide films using atomic layer deposition (ALD). This process creates conformal films of controllable thickness on each fiber, while providing a more reactive surface for MOF nucleation. By submerging the ALD coated fabric in solution during solvothermal MOF synthesis, the MOFs create a conformal, well-adhered coating on the fibers, resulting in a MOF-functionalized fabric, without additional adhesion materials that may block MOF pores and functional sites. Here we demonstrate two solvothermal synthesis methods. First, we form a MIL-96(Al) layer on polypropylene fibers using synthetic conditions that convert the metal oxide to MOF. Using initial inorganic films of varying thicknesses, diffusion of the organic linker into the inorganic allows us to control the extent of MOF loading on the fabric. Second, we perform a solvothermal synthesis of UiO-66-NH_2 in which the MOF nucleates on the conformal metal oxide coating on polyamide-6 (PA-6) fibers, thereby producing a uniform and conformal thin film of MOF on the fabric. The resulting materials can be directly incorporated into filter devices or protective clothing and eliminate the maladroit qualities of loose powder.

Video Link

The video component of this article can be found at https://www.jove.com/video/57734/

Introduction

Metal-organic frameworks are crystalline structures consisting of reactive metal cluster centers bridged by organic molecule linkers to provide large porosities and surface areas. Their structure, porosity, and functionality can be designed by choosing appropriate clusters and linkers, leading to surface areas as high as 7,000 m^2/g_{MOF}[1,2]. Their high porosity and surface area have made MOFs diversely applicable in adsorption, separation, and heterogeneous catalysis in fields ranging from energy production to environmental concerns to biological processes[1,3,4,5,6].

Numerous MOFs have proven successful in selectively adsorbing volatile organic compounds and greenhouse gases or to catalytically degrade chemicals that may prove harmful to human health or the environment. In particular, MIL-96 (Al) has shown to selectively adsorb nitrogenous volatile organic compounds (VOCs) due to the availability of lone pair electrons in the nitrogen groups to coordinate with the weak Lewis acid Al present in the metal clusters[7]. MIL-96 has also been shown to adsorb gases such as CO_2, *p*-xylene, and *m*-xylene[8,9]. MOF adsorption selectivity is dependent on both the Lewis acid of the metal cluster, as well as pore size. The pore size of MIL-96 increases with temperature, resulting in increased adsorption capacity of trimethylbenzene with increased temperature, and presents the opportunity of tuning selectivity with adsorption temperature[9].

The second MOF of focus here, UiO-66-NH_2 has been shown to catalytically degrade chemical warfare agents (CWAs) and simulants. The amine group on the linker provides a synergistic effect in degrading nerve agents, while preventing agent degradation products from binding irreversibly to the zirconium clusters and poisoning the MOF[10]. UiO-66-NH_2 has catalytically hydrolyzed dimethyl *p*-nitrophenylphosphate (DMNP) with a half-life as short as 0.7 minutes in buffered conditions, nearly 20 times faster than its base MOF UiO-66[11,12].

While these adsorption and catalytic properties are promising, the physical form of the MOFs, primarily bulk powder, can be difficult to incorporate into platforms for gas capture and filtration without adding significant bulk, clogging pores, or reducing MOF flexibility. An alternative is to create MOF functionalized fabrics. MOFs have been incorporated into fabrics in myriad ways, including electrospinning MOF powder/polymer slurries, adhesive mixes, spray coating, solvothermal growth, microwave syntheses, and a layer-by-layer growth method[13,14,15,16,17,18]. Of these, electrospinning and polymer adhesives can result in blocked functional sites on the MOF as they are encapsulated in the polymer, significantly decreasing adsorption capacity and reactivity. Additionally, many of these techniques fail to create conformal coatings on the fibers due to line of sight difficulties or poor adhesion/nucleation and the reliance on purely electrostatic interactions. An alternative method is to first coat the fabric with a metal oxide to allow for stronger surface interactions with the MOF[18,19].

Copyright © 2018 Journal of Visualized Experiments

One method of metal oxide deposition is atomic layer deposition (ALD). ALD is a technique for depositing conformal thin films, controllable to the atomic scale. The process utilizes two half reactions that occur only at the surface of the substrate to be coated. The first step is to dose a metal containing precursor, which reacts with hydroxyls on the surface, leaving a metallated surface while excess reactant is purged from the system. The second reactant is an oxygen-containing reactant, typically water, which reacts with the metal sites to form a metal oxide. Again, excess water and any reaction products are purged from the system. These alternating doses and purges can be repeated until the desired film thickness is achieved (**Figure 1**). Atomic layer deposition is particularly useful because the small-scale vapor phase precursors allow for conformal films on every surface of substrates with complex topology, such as fiber mats. Additionally, for polymers such as polypropylene, the ALD conditions can allow the coating to diffuse into the fiber surface, providing a strong anchor for future MOF growth[20].

The metal oxide coating allows for increased nucleation sites on the fibers during traditional solvothermal synthesis by increasing functional groups and roughness[18,20]. Our group has previously shown the ALD metal oxide base layer is effective for UiO-6X, HKUST-1, and other syntheses through various routes of solvothermal, layer-by-layer, and hydroxy-double salt conversion methods[13,17,18,21,22,23]. Here we demonstrate two synthesis types. The MIL materials are formed by converting the Al_2O_3 ALD coating directly to MOF by diffusion of the organic linker. By submerging an Al_2O_3 ALD coated fiber mat in trimesic acid solution and heating, the organic linker diffuses into the metal oxide coating to form MIL-96. This results in a strongly adhered, conformal MOF coating on every fiber surface. The second synthesis approach calls for typical UiO-66-NH_2 hydrothermal synthesis using metal and organic precursors, but adds a metal oxide coated fiber mat on which the MOF nucleates. For both synthesis approaches, the resulting products consist of conformal thin films of MOF crystals strongly adhered to the supporting fabric. In the case of MIL-96, these can be incorporated into filters for adsorption of VOCs or greenhouse gases. For UiO-66-NH_2 these fabrics can be easily incorporated into lightweight protective clothing for military personnel, first responders, and civilians for continuous defense against CWA attacks.

Protocol

1. Atomic Layer Deposition (ALD) of Al_2O_3 on Fiber Mats

1. Place a 2.54 x 2.54 cm^2 polypropylene fabric sample in the reactor boat (a thin, rigid, metal mesh holder). A schematic of the reactor is presented in **Figure 2**.
2. Open the pressure gauge. Remove the clasp from the reactor cap. Turn on manual control in the LabView system. Close the carrier nitrogen and gate valve on the ALD reactor. Open the vent nitrogen.
3. After removing the reactor cap, load the fabric sample into the ALD reactor. Replace the reactor cap and open the gate valve. Close the vent and open the carrier nitrogen. Turn off manual control.
4. Load the recipe for Al_2O_3 on fabrics. The recipe will alternately dose trimethylaluminum (TMA) for 1.2 s, followed by a 30 s dry nitrogen purge or dose water for 1 s followed by a 60 s dry nitrogen purge. Set the recipe to run 1000 cycles.
5. Set the mass flow controller to 20 cfm and the furnace temperature to 90 °C (84 °C on the furnace interface).
6. Open the manual valve to the TMA and water. Close the pressure gauge. Replace the clasp on the reactor cap. Press **Start** on the interface.
7. Upon completion of the recipe, open the pressure gauge. Remove the clasp from the reactor cap. Turn on manual control in the system. Close the carrier nitrogen and gate valve on the ALD reactor. Open the vent nitrogen.
8. Remove the reactor cap and sample boat. Re-seal the reactor.
   NOTE: The procedure may be paused at this point.

2. Atomic Layer Deposition (ALD) of TiO_2 on Polyamide-6 (PA-6) Fiber Mats

1. Place a 2.54 x 2.54 cm^2 PA-6 fabric sample in the reactor boat (a thin, rigid, metal mesh holder).
2. Open the pressure gauge. Remove the clasp from the reactor cap. Turn on manual control in the LabView system. Close the carrier nitrogen and gate valve on the ALD reactor. Open the vent nitrogen.
3. After removing the reactor cap, load the fabric sample into the ALD reactor. Replace the reactor cap and open the gate valve. Close the vent and open the carrier nitrogen. Turn off manual control.
4. Load the recipe for TiO_2 on fabrics. The recipe will alternately dose $TiCl_4$ for 1 s, followed by a 40 s dry nitrogen purge or dose water for 1 s followed by a 60 s dry nitrogen purge. Set the recipe to run 300 cycles.
5. Set the mass flow controller to 20 cfm and the furnace temperature to 90 °C (84 °C on the furnace interface).
6. Open the manual valve to the $TiCl_4$ and water. Close the pressure gauge. Replace the clasp on the reactor cap. Press **Start** on the interface.
7. Upon completion of the recipe, open the pressure gauge. Remove the clasp from the reactor cap. Turn on manual control in the system. Close the carrier nitrogen and gate valve on the ALD reactor. Open the vent nitrogen.
8. Remove the reactor cap and sample boat. Re-seal the reactor.
   NOTE: The procedure may be paused at this point.

3. Solvothermal Synthesis of MIL-96

1. Add 0.0878 g of H_3BTC to an 80 mL glass beaker.
2. Add 12 mL of H_2O and 12 mL of ethanol to the beaker.
3. Stir magnetically for 10 min or until the H_3BTC is fully dissolved.
4. Place the solution in a Teflon lined pressure vessel.
5. Add the Al_2O_3 coated polypropylene to the solution and prop the fabric on a mesh support so it does not lie flat against the bottom of the vessel.
6. Seal the pressure vessel and place it in the furnace at 110 °C for 24 h.
7. After allowing the sample to cool, place the fabric sample in a mesh basket in a beaker. Wash twice with ethanol, each for 12 h.
8. Sample activation requires heating at 85 °C for 6 h under vacuum, followed by heating at 110 °C for 12 h under vacuum.

Copyright © 2018 Journal of Visualized Experiments

NOTE: The procedure can be stopped here. All samples should be stored in a desiccator to maintain sample activation.

4. Solvothermal Synthesis of UiO-66-NH_2

1. Add 0.08 g of $ZrCl_4$ to a 20 mL glass scintillation vial.
2. Add 20 mL of N,N-dimethylformamide (DMF) to the $ZrCl_4$ in 5 mL increments. Cap the vial between increments and allow fumes to dissipate.
3. Sonicate the solution for 1 min.
4. Add 0.062 g of 2-aminoterephthalic acid to the vial, and magnetically stir the solution for 5 min.
5. Add 25 µL of deionized water to the vial.
6. Add 1.33 mL of concentrated HCl to the vial.
7. Submerge the TiO_2 ALD coated fabric swatch in the solution and cap the vial.
8. Place the sample in the furnace at 85 °C for 24 h.
9. After allowing the sample to cool, place the fabric sample in a mesh basket in a beaker. Wash twice with 80 mL of DMF, each for 12 h. Wash 3 times with 80 mL of ethanol, each for 12 h.
10. After removing the fabric swatch, filter the residual MOF powder. Wash twice with 80 mL of DMF, each for 12 h. Wash 3 times with 80 mL of ethanol, each for 12 h.
11. Sample activation requires heating at 85 °C for 6 h under vacuum, followed by heating at 110 °C for 12 h under vacuum.
    NOTE: The procedure can be stopped here. All samples should be stored in a desiccator to maintain sample activation.

Representative Results

To describe the MOF/fabric materials, we delineate two terms related to measured surface area. First, projected surface area, $cm^2_{projected}$, refers to the macroscopic size of the fabric swatch as measured with a ruler, *i.e.*, the area of the sample's projected shadow. The second surface area of interest is the BET surface area, calculated from a nitrogen isotherm obtained at 77 K. These values are given in units of m^2/g_{Fabric}, m^2/g_{MOF}, or $m^2/g_{MOF+Fabric}$, corresponding respectively to the measured or estimated total surface area per gram of sample for the fabric before MOF loading, the MOF itself, or the fabric after loading with MOF. For ALD coated fabrics and MIL-96 coated fabrics, the surface areas were calculated from a partial pressure range of 0.05 to 0.3. For samples containing UiO-66-NH_2, surface areas were calculated using a partial pressure range of 0.02 to 0.08, due to the presence of microporosity. All samples had correlation coefficients of 0.995 or higher. Fit parameters are listed for each sample in **Table 1**. The specific surface area of a MOF on fabric, m^2/g_{MOF}, is calculated using measured mass and surface area of MOF on fabric:

$$m^2/g_{MOF} = \frac{(m^2/g_{MOF+Fabric}) - (m^2/g_{Fabric})}{(g_{MOF+Fabric} - g_{Fabric})}.$$

After coating fabrics with 1000 cycles of Al_2O_3 ALD, the polypropylene fabric appeared visually unchanged, although some additional stiffness could be felt by hand. Ellipsometry of monitor silicon wafers revealed 1100 ±15 Å of Al_2O_3 growth using a Cauchy model. The ALD coating resulted in a mass gain of 1.16 $mg_{Al2O3}/cm^2_{projected}$. This process was repeated with 500 and 2000 cycles of Al_2O_3, resulting in 600 ±15 and 2010 ±40 Å on the monitor silicon wafers. The mass increase was 0.65 $mg_{Al2O3}/cm^2_{projected}$ and 2.26 $mg_{Al2O3}/cm^2_{projected}$ on the 500 and 2000 cycle samples respectively. The BET surface area of the Al_2O_3(1000) coated polypropylene was 4.7 m^2/g_{Fabric}.

Following the MOF synthesis, the resulting solution was clear and free of loose MOF powder, indicating strong MOF and ALD adhesion on the fiber. After washing and drying, the sample mass increase on the 500, 1000, and 2000 cycle samples was 40, 73, and 77% of the mass of the initial samples, respectively. Parallel exposure of Al_2O_3 coated fabric samples to synthesis conditions in the absence of MOF linker or metal-cluster precursors revealed an inherent mass gain of 10-20%, suggesting the mass measurements exaggerate the MOF loading. Examination with scanning electron microscopy (SEM) showed conformal MOF crystal thin films on all fibers, resembling a cobblestone pattern (**Figure 3b–3c**). When the Al_2O_3 was reduced to 500 cycles, the film began to break apart as the MOF formed, resulting in a patchy coating (**Figure 3a**). A bare polypropylene sample with no Al_2O_3 coating was also exposed to MIL-96 synthesis conditions (**Figure 3d**), but XRD showed no detectable MOF present on the fibers. Cross-sectional images of these samples revealed the 500 cycle Al_2O_3 base layer completely reacted, while a fraction of the Al_2O_3 base layer remained for the 1000 and 2000 cycle samples (**Figure 4d–4f**). Cross-sections of the original Al_2O_3 ALD coated polypropylene are shown in **Figure 4a-4c**. In the 24 hour reaction time, approximately 80±20 nm of Al_2O_3 reacted or was potentially etched away in the acidic synthesis conditions. Electron dispersion spectroscopy images of the cross-section revealed the carbon based polypropylene core and predominantly Al_2O_3 shell (**Figure 5**). X-ray diffraction patterns of the MOF coated fabric, matching the simulated PXRD pattern of MIL-96, are shown in **Figure 6**. The measured surface area after MOF growth was 6.0 $m^2/g_{MOF+Fabric}$, 6.7 $m^2/g_{MOF+Fabric}$, and 19.9 $m^2/g_{MOF+Fabric}$, for the 500, 1000, and 2000 cycle samples respectively. Adsorption and desorption isotherms are shown in **Figure 7**.

The PA-6 fiber mats appeared slightly yellowed after deposition of 300 cycles of TiO_2, but the mat felt nearly unchanged in stiffness. Ellipsometry revealed 175 ±15 Å of TiO_2 for ALD at 50, 90, or 200 °C on the monitor silicon. The ALD mass loading was 0.17, 0.20, and 0.25 $mg_{TiO2}/cm^2_{projected\ area\ PA\text{-}6}$ for the 50, 90, and 200 °C samples. The BET surface area of the PA-6 fabric coated with 300 cycles of TiO_2 at 90 °C was 8.2 m^2/g_{Fabric}.

Copyright © 2018 Journal of Visualized Experiments

Following solvothermal MOF synthesis, XRD patterns revealed UiO-66-NH_2 was present on the fibers (**Figure 8**). The MOF mass gain on the 50, 90, and 200 °C samples was 2.4, 78, and 0%. A parallel exposure of TiO_2 coated nylon to synthesis conditions in the absence of MOF metal-cluster or linker precursors revealed a mass gain of 10-20%. Additionally, fabric was easily torn during the MOF synthesis and the acidic conditions may etch the TiO_2 film, leading to uncertainties in the MOF loading. SEM images showed the MOF coatings on each sample, with flaky coatings on the 50 °C samples, dense coatings on the 90 °C samples, and sparse coatings on the 200 °C samples (**Figure 9a–9c**). An uncoated PA-6 sample was also exposed to UiO-66-NH_2 synthesis conditions, resulting in a relatively sparse coating of MOF crystals (**Figure 9d**). The measured BET surface areas after MOF synthesis were 16.0 $m^2/g_{MOF+Fabric}$, 19.8 $m^2/g_{MOF+Fabric}$, and 4.67 $m^2/g_{MOF+Fabric}$, for the 50, 90, and 200 °C samples respectively. Adsorption and desorption isotherms are shown in **Figure 10**.

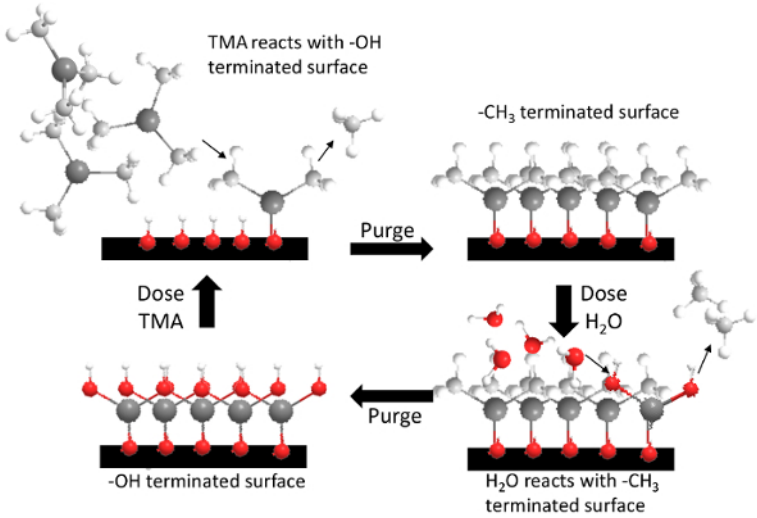

Figure 1. Schematic of Al_2O_3 ALD process: In the first step, precursor dosing, trimethyl aluminum precursor reacts with the hydroxyl terminated surface. The excess precursor is then purged from the system, resulting in a uniform aluminum-dimethyl terminated surface. During the water dose step the water reacts to replace the methyl groups, resulting in a newly hydroxyl terminated surface. In the last step of the cycle, the excess water is purged from the system. Please click here to view a larger version of this figure.

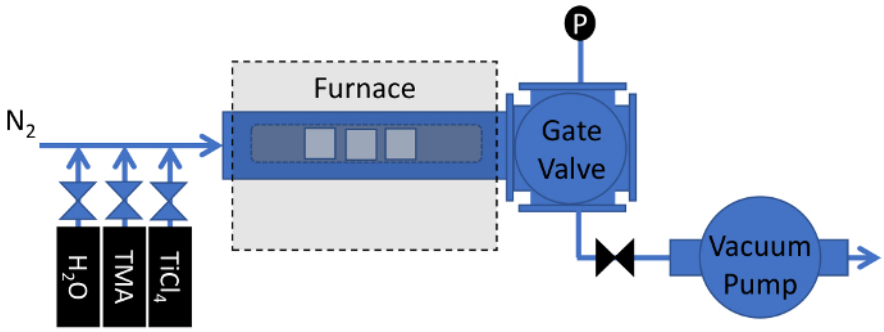

Figure 2. ALD reactor schematic: The system is a home-built, hot-walled viscous flow reactor with a dry nitrogen carrier gas. The precursor lines are wrapped with heat tape, while the actual deposition zone holding the mesh sample boat is located within a furnace. The system is operated under vacuum at ~1.8 Torr. Please click here to view a larger version of this figure.

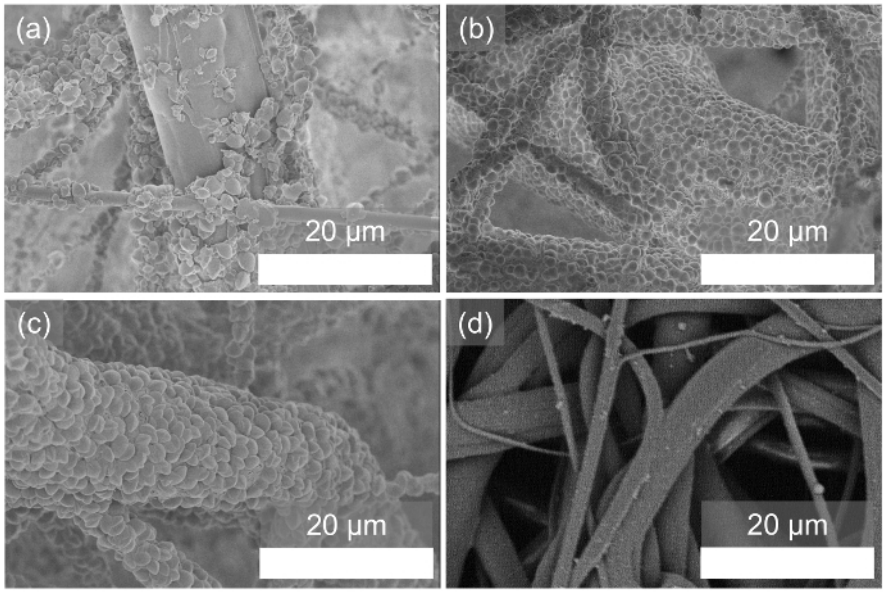

Figure 3. SEM images of PP with **(a)** Al_2O_3(500)/MIL-96, **(b)** Al_2O_3(1000)/MIL-96, **(c)** Al_2O_3(2000)/MIL-96, and **(d)** no ALD coating after exposure to the MIL-96 synthesis conditions. Please click here to view a larger version of this figure.

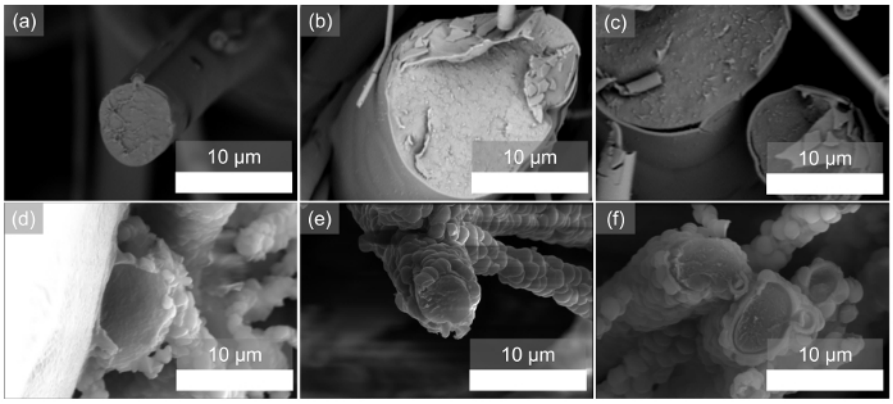

Figure 4. SEM images of the cross-section of PP with **(a)** Al_2O_3 (500), **(b)** Al_2O_3 (1000), **(c)** Al_2O_3 (2000), **(d)** Al_2O_3 (500)/MIL-96, **(e)** Al_2O_3 (1000)/MIL-96, **(f)** Al_2O_3 (2000)/MIL-96. Please click here to view a larger version of this figure.

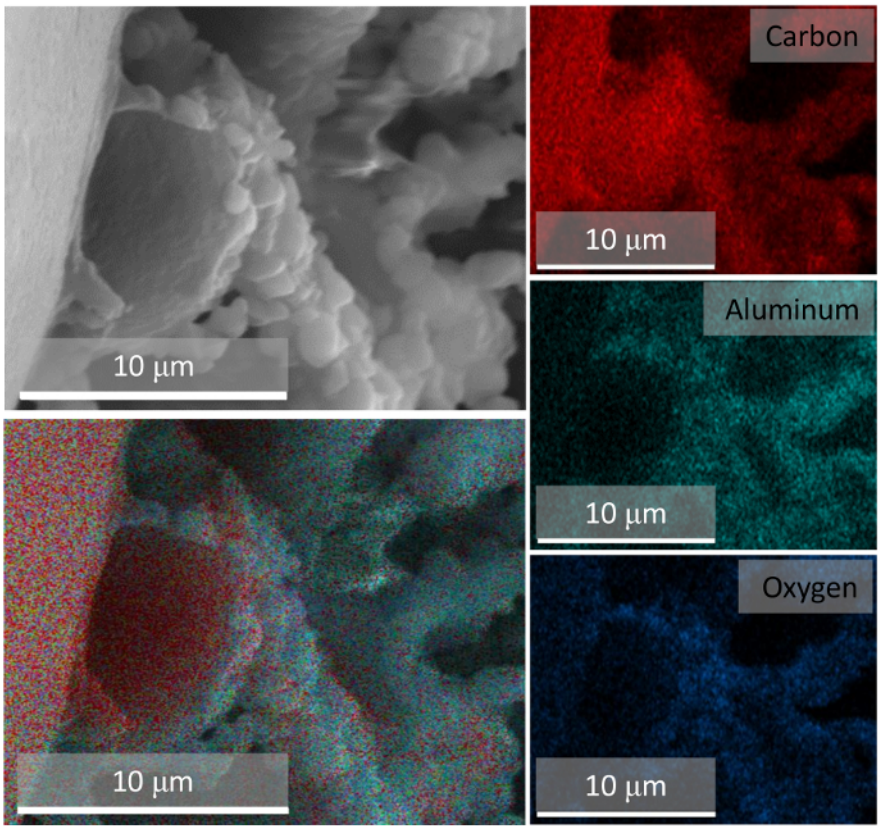

Figure 5. EDS images of the cross-section of PP/Al_2O_3 (500)/MIL-96 reveals the carbon based polypropylene core with the predominantly Al_2O_3 shell. Please click here to view a larger version of this figure.

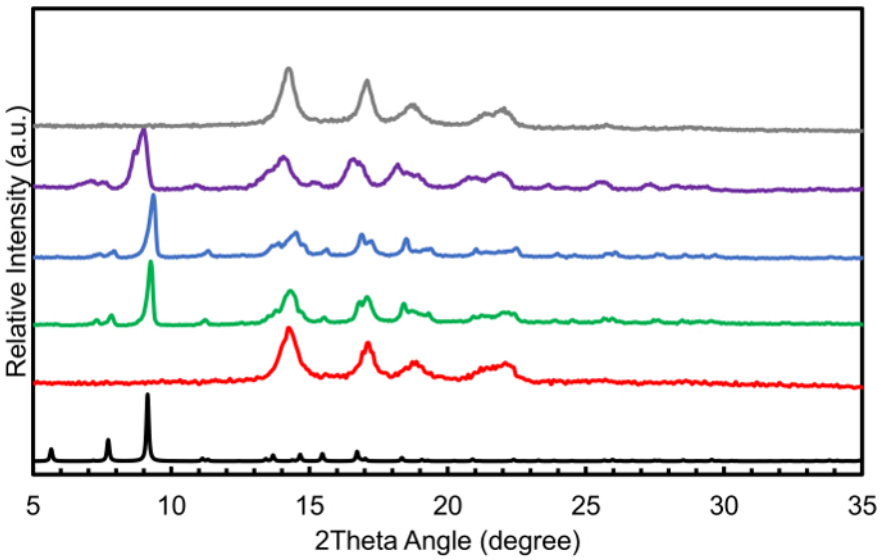

Figure 6. (black) Simulated PXRD pattern of MIL-96, **(red)** XRD pattern of Al_2O_3 coated polypropylene, **(green)** MIL-96 on Al_3O_3 (500) coated polypropylene, **(bue)** MIL-96 on Al_3O_3 (1000) coated polypropylene, **(purple)** MIL-96 on Al_3O_3 (2000) coated polypropylene and **(gray)** bare PP after exposure to MIL-96 synthesis conditions. Please click here to view a larger version of this figure.

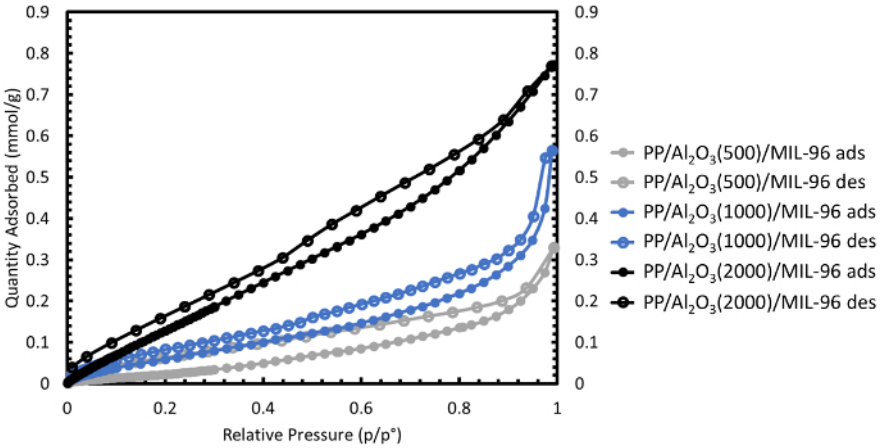

Figure 7. (grey) N_2 adsorption and desorption isotherms for MIL-96 on 500 cycles of Al_2O_3 on polypropylene **(blue)** adsorption and desorption isotherms for MIL-96 on 1000 cycles of Al_2O_3 on polypropylene **(black)** adsorption and desorption isotherms for MIL-96 on 2000 cycles of Al_2O_3 on polypropylene. Please click here to view a larger version of this figure.

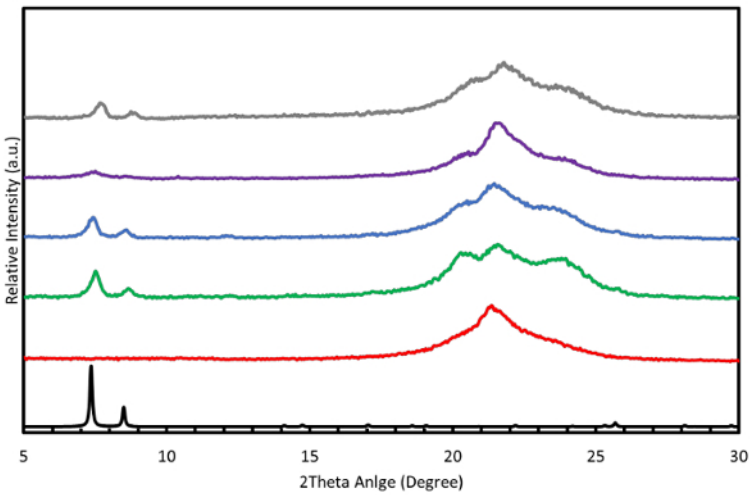

Figure 8. (black) Simulated PXRD pattern of UiO-66-NH_2, **(red)** XRD pattern of TiO_2 coated PA-6, **(green)** UiO-66-NH_2 on TiO_2(50 °C), coated PA-6 **(blue)** UiO-66-NH_2 on TiO_2(90 °C) coated PA-6, **(purple)** UiO-66-NH_2 on TiO_2(200 °C) coated PA-6 and **(gray)** UiO-66-NH_2 on bare PA-6. Please click here to view a larger version of this figure.

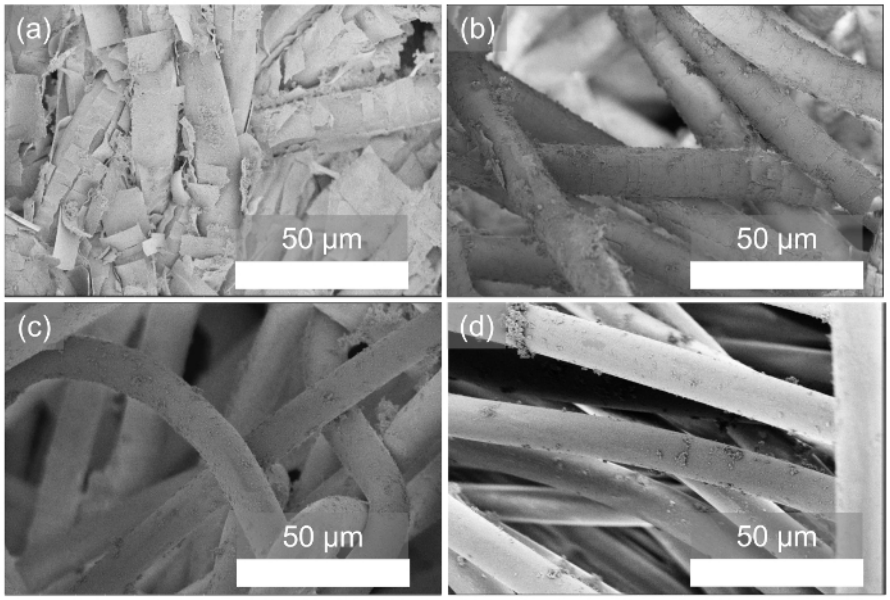

Figure 9. SEM images of PA-6/TiO_2/UiO-66-NH_2 with ALD deposition at (**a**) 50 °C, (**b**) 90 °C and (**c**) 200 °C and (**d**) UiO-66-NH_2 on PA-6 with no ALD base coat, demonstrating the higher ALD temperature results in greater diffusion of the ALD precursors into the fiber, altering the MOF adhesion. Please click here to view a larger version of this figure.

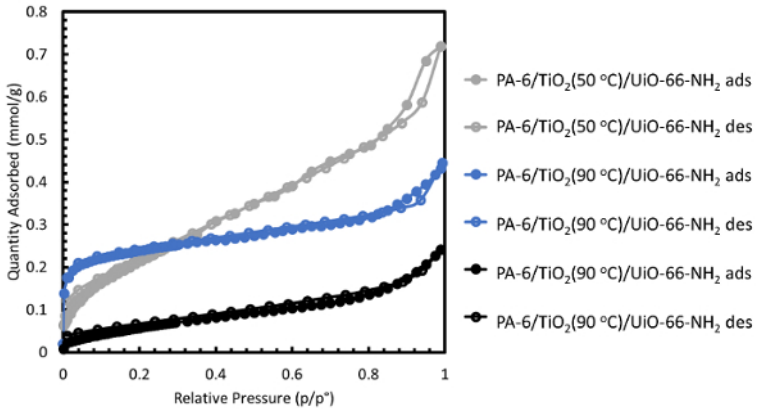

Figure 10. N_2 Adsorption and desorption isotherms for PA-6/TiO_2/UiO-66-NH_2 with ALD deposition at **(grey)** 50 °C **(blue)** 90 °C, and **(black)** 200 °C. Please click here to view a larger version of this figure.

Sample	C	Y (g/mmol)	Slope (g/mmol)	Qm (mmol/G)
PP/Al_2O_3 (1000)	6.61	3.13	17.59	0.048
PP/Al_2O_3 (500)/MIL-96	7.01	2.31	13.588	0.062
PP/Al_2O_3 (1000)/MIL-96	9.24	1.58	13.01	0.069
PP/Al_2O_3 (2000)/MIL-96	4.06	1.21	3.69	0.2
Nylon/TiO_2 (90 °C)	2.99	3.97	10.57	0.072
Nylon/TiO_2 (50 °C)/UiO-66-NH_2	63.09	0.096	5.99	0.16
Nylon/TiO_2 (90 °C)/UiO-66-NH_2	599	0.0082	4.92	0.2
Nylon/TiO_2 (200 °C)/ UiO-66-NH_2	32.43	0.644	20.24	0.048

Table 1. List of BET fit parameters for each sample.

Discussion

The ALD coating strongly influences the adhesion and loading of the MOF. First, depending on the type of substrate and ALD precursor, the ALD layer can either form a distinct outer shell around the fiber, or diffuse into the fiber to create a gradual transition to the metal oxide coating[20]. The hard shell has been observed on cotton and nylon substrates, while diffusive layers can be observed in polypropylene under proper conditions. Second, the diffusion into the fiber can also be controlled by varying the deposition temperature[20,24]. Higher temperatures increase the diffusion of the ALD precursors into the fiber. Lastly, the metal oxide coating must be thick enough after diffusion to form a conformal outer coating and provide functional groups and increased surface roughness for the MOF to nucleate[18,20]. While silicon wafers were used to monitor the ALD growth and estimate film thickness, polymer spin-coated on QCM crystals can serve as a more accurate means to track mass uptake, coupled with FTIR intensities to estimate film thicknesses[24]. These methods would require more time and materials, but could account for delayed or accelerated nucleation on polymer films, rather than estimating based on the ALD growth on silicon. Alternatively, TEM cross-sectional imaging could be used, but this may result in breaking or compressing the fiber coatings.

Unlike conventional MOF synthesis, the MIL synthesis relies on a metal source anchored on a fiber. Under proper conditions, the Al_2O_3 coating on polypropylene can diffuse into the fiber, helping to anchor the MOF after synthesis. However, if the metal oxide is fully reacted or if the ALD diffusion is limited, the adhesive forces may be slightly diminished. An example of this is present for the MIL-96 grown using 500 ALD cycles of Al_2O_3, as shown in the SEM image in **Figure 3a**. The patchy MOF coverage and loose fragments are evidence of the MOF layer peeling away from the fiber after the metal oxide has been fully reacted, confirmed by the cross-sectional images in **Figure 4**. For the thicker metal oxide layers, this peeling is not observed. The MOF loading of the MIL is limited by the metal source on the fiber. The MOF loading on the 500 cycle sample was likely low because the Al was fully consumed. The uniform MOF adhesion on the 1000 cycle and 2000 cycle samples, and their cross-sectional images, suggest the Al_2O_3 was not fully consumed. The loading was limited by the diffusion rate of the trimesic acid organic linker into the Al_2O_3 and longer synthesis time may reveal a higher MOF loading on the thicker Al_2O_3 coatings.

Separately from the MOF syntheses on fabrics, Al_2O_3 powder was used in place of the Al_2O_3 ALD coating during a MIL-96 synthesis. The powder did not react. To understand the difference in reactivity between the powder and film, the dielectric constants were compared. Using ellipsometry measurements on the film, the refractive index was found to be 1.63, giving a dielectric constant of 2.66, while the literature value of Al_2O_3 is 10[25]. This suggests the ALD film is much more likely to form a dipole, making it more reactive. Given the low ALD temperature, this is likely due to hydroxyls remaining in the film creating defects.

The 2000 cycle samples had the highest BET surface area, consistent with a larger mass loading than on the 500 cycle samples. The smaller BET surface area of the MIL-96 on the fibers coated with 500 ALD cycles reflects the small mass loading. The literature value for the BET surface area of synthesized MIL-96 is approximately 600 m^2/g_{MOF}[7,8]. Using the mass measurements and surface areas, the calculated specific surface area of MIL on fabrics was only one tenth of the literature values, though this is improved with thicker ALD base layers. This estimate may be artificially low due to exaggerated mass measurements and insufficient material in the BET.

For the UiO-66-NH_2 synthesis, the TiO_2 on PA-6 fibers interacts with the backbone of the fiber to change the structural properties while also forming a hard outer shell on the microfibers[20,26]. The coatings deposited at 50 °C resulted in pealing and poor adhesion after MOF synthesis because the low temperature limited the diffusion of the precursor into the fiber. For metal oxides deposited at 90 °C, this peeling was largely eliminated due to the increased temperature of deposition, though some cracks can still be observed in the film. At 200 °C, the diffusion into the fiber eliminated peeling and cracking, but at the expense of thinning the available TiO_2 at the surface of the fiber. The thick outer shells deposited at 50 and 90 °C still resulted in MOF growth, but the MOF growth was very limited on TiO_2 deposited at 200 °C, likely because the outermost shell is so thin. The BET surface area of these samples reflects the growth on the TiO_2 layers. The UiO-66-NH_2 powder surface area was 1325 m^2/g_{MOF}, in agreement with literature reported values. Back calculating the MOF surface area from the mass measurements and sample surface areas reveals the MOF powders on fabrics had at best half the surface area per gram MOF. In all cases, while the mass loadings could be misleading, the thicker outer ALD layers correlated to larger BET surface areas post MOF growth, possibly resulting in better MOF crystallinity as the MOF precursors interacted less with the fibers.

Future studies may examine atomic layer deposition for a variety of metal oxides, including ZnO, ZrO_2, and HfO_2, which may be applicable for alternative MOF syntheses[27]. However, some of these processes require much higher deposition temperatures, limiting feasible fabrics for deposition. Additionally, MOFs with much more complex metal centers, such as Zr_6 clusters, may be much more difficult to achieve due to the limited mobility of the film. However, in choosing appropriate ALD precursors and temperatures, fluidity of the film may be achieved at higher MOF synthesis temperatures[28].

Disclosures

The authors have nothing to disclose.

Acknowledgements

The authors thank their collaborators at RTI International, US Army Natick Soldier RD&E Center, and Edgewood Chemical and Biological Center. They also thank their funding source, the Defense Threat Reduction Agency.

References

1. Furukawa, H., Cordova, K. E., O'Keeffe, M., & Yaghi, O. M. The Chemistry and Applications of Metal-Organic Frameworks. *Science (Washington, DC, U. S.).* **341** (6149), 974 (2013).

2. Farha, O. K. *et al.* Metal−Organic Framework Materials with Ultrahigh Surface Areas: Is the Sky the Limit? *Journal of the American Chemical Society.* **134** (36), 15016-15021 (2012).
3. Bobbitt, N. S. *et al.* Metal-organic frameworks for the removal of toxic industrial chemicals and chemical warfare agents. *Chemical Society Reviews.* **46** (11), 3357-3385 (2017).
4. Prawiec, P. *et al.* Improved Hydrogen Storage in the Metal-Organic Framework Cu3(BTC)2. *Advanced Engineering Materials.* **8** (4), 293-296 (2006).
5. Moon, S.-Y. *et al.* Effective, Facile, and Selective Hydrolysis of the Chemical Warfare Agent VX Using Zr6-Based Metal-Organic Frameworks. *Inorganic Chemistry.* **54** (22) 10829-10833 (2015).
6. Zhou, H. & Kitagawa, S. Metal-Organic Frameworks (MOFs). *Chemical Society Reviews.* **43** (16), 5415-5418 (2014).
7. Qiu, M., Chen, C., & Li, W. Rapid controllable synthesis of Al-MIL-96 and its adsorption of nitrogenous VOCs. *Catalysis Today.* **258,** 132-138 (2015).
8. Abid, H. R., Rada, Z. H., Shang, J., & Wang, S. Synthesis, characterization, and CO2 adsorption of three metal-organic frameworks (MOFs): MIL-53, MIL-96, and amino-MIL-53. *Polyhedron.* **120,** 103-111 (2016).
9. Lee, J. S., & Jhung, S. H. Vapor-phase adsorption of alkylaromatics on aluminum-trimesate MIL-96: An unusual increase of adsorption capacity with temperature. *Microporous Mesoporous Materials.* **129** (1-2), 274-277 (2010).
10. Gil-San-Millan, R. *et al.* Chemical Warfare Agents Detoxification Properties of Zirconium Metal-Organic Frameworks by Synergistic Incorporation of Nucleophilic and Basic Sites. *ACS Appl. Material Interfaces.* **9** (28), 23967-23973 (2017).
11. Peterson, G. W. *et al.* Tailoring the Pore Size and Functionality of UiO-Type Metal-Organic Frameworks for Optimal Nerve Agent Destruction. *Inorganic Chemistry.* **54** (20), 9684-9686 (2015).
12. Katz, M. J. *et al.* Exploiting parameter space in MOFs: a 20-fold enhancement of phosphate-ester hydrolysis with UiO-66-NH2. *Chemical Science.* **6** (4), 2286-2291 (2015).
13. Zhao, J. *et al.* Highly Adsorptive, MOF-Functionalized Nonwoven Fiber Mats for Hazardous Gas Capture Enabled by Atomic Layer Deposition. *Advanced Materials Interface.* **1** (4), 1400040 (2014).
14. Peterson, G. W., Lu, A. X., & Epps, III, T. H. Tuning the Morphology and Activity of Electrospun Polystyrene/ UiO-66-NH2 Metal-Organic Framework Composites to Enhance Chemical Warfare Agent Removal. *ACS Applied Materials & Interfaces.* **9** (37), 32248-32254 (2017).
15. Lee, D. T., Zhao, J., Peterson, G. W., & Parsons, G. N. Catalytic ' MOF-Cloth ' Formed via Directed Supramolecular Assembly of UiO-66-NH 2 Crystals on Atomic Layer Deposition- Coated Textiles for Rapid Degradation of Chemical Warfare Agent Simulants. *Chemistry of Materials.* **29** (11), 4894-4903 (2017).
16. López-maya, E. *et al.* Textile / Metal - Organic-Framework Composites as Self-Detoxifying Filters for Chemical-Warfare Agents. *Angewandte Chemie International Edition.* **54** (23), 6790-6794 (2015).
17. Zhao, J. *et al.* Conformal and highly adsorptive metal-organic framework thin films via layer-by-layer growth on ALD-coated fiber mats. *Journal of Materials Chemistry. A.* **3** (4), 1458-1464 (2015).
18. Lemaire, P. C. *et al.* Copper Benzenetricarboxylate Metal-Organic Framework Nucleation Mechanisms on Metal Oxide Powders and Thin Films formed by Atomic Layer Deposition. *ACS Applied Materials & Interfaces.* **8** (14), 9514-9522 (2016).
19. Zacher, D., Baunemann, A., Hermes, S., & Fischer, R. A. Deposition of microcrystalline [Cu3(btc)2] and [Zn2(bdc)2(dabco)] at alumina and silica surfaces modified with patterned self assembled organic monolayers: evidence of surface selective and oriented growth. *Journal of Materials Chemistry.* **17** (27), 2785-2792 (2007).
20. Parsons, G. N. *et al.* Mechanisms and reactions during atomic layer deposition on polymers. *Coordination Chemisty Reviews.* **257** (23-24), 3323-3331 (2013).
21. Zhao, J. *et al.* Facile Conversion of Hydroxy Double Salts to Metal-Organic Frameworks Using Metal Oxide Particles and Atomic Layer Deposition Thin-Film Templates. *Journal of the American Chemical Soceity.* **137** (43), 13756-13759 (2015).
22. Zhao, J. *et al.* Ultra-Fast Degradation of Chemical Warfare Agents Using MOF - Nanofiber Kebabs. *Angewandte Chemie International Edition.* **55** (42), 13224-13228 (2016).
23. Lee, D., Zhao, J., Oldham, C., Peterson, G., & Parsons, G. UiO-66-NH2 Metal–Organic Framework (MOF) Nucleation on TiO2, ZnO, and Al2O3 Atomic Layer Deposition-Treated Polymer Fibers: Role of Metal Oxide on MOF Growth and Catalytic Hydrolysis of Chemical Warfare Agent Simulants. *ACS Applied Materials & Interfaces.* **9** (51), 44847-44855 (2017).
24. Spagnola, J. C. *et al.* Surface and sub-surface reactions during low temperature aluminium oxide atomic layer deposition on fiber-forming polymers. *Journal of Materials Chemistry.* **20** (20), 4213-4222 (2010).
25. Nalwa, H. S. *Handbook of low and high dielectric constant materials and their applications.* Academic Press (1999).
26. Mcclure, C., Oldham, C., Walls, H., & Parsons, G. Large effect of titanium precursor on surface reactivity and mechanical strength of electrospun nanofibers coated with TiO2 by atomic layer deposition. *Journal of Vacuum Science and Technology A.* **31** (6), 61506 (2013).
27. Johnson, R. W., Hultqvist, A., & Bent, S. F. A brief review of atomic layer deposition: from fundamentals to applications. *Materials Today.* **17** (5), 236-246 (2014).
28. Stassen, I., Vos, D. De, & Ameloot, R. Vapor-Phase Deposition and Modification of Metal - Organic Frameworks : State-of-the-Art and Future Directions. *Chemistry: A European Journal.* **22** (41), 14452-14460 (2016).

Copyright © 2018 Journal of Visualized Experiments